

## Reconstructing marine redox conditions for the transition between Cambrian Series 2 and Cambrian Series 3, Kaili area, Yangtze Platform: Evidence from biogenic sulfur and degree of pyritization



Qingjun Guo <sup>a,\*</sup>, Harald Strauss <sup>b</sup>, Yuanlong Zhao <sup>c</sup>, Xinglian Yang <sup>c</sup>, Jin Peng <sup>c</sup>, Yuning Yang <sup>c</sup>, Yinan Deng <sup>a</sup>

<sup>a</sup> Center for Environmental Remediation, Institute of Geographic Sciences and Natural Resources Research, Chinese Academy of Sciences, Beijing 100101, China

<sup>b</sup> Institut für Geologie und Paläontologie, Westfälische Wilhelms-Universität Münster, Corrensstrasse 24, 48149 Münster, Germany

<sup>c</sup> Institute of Resource and Environmental Engineering, Guizhou University, Guiyang 550002, China

### ARTICLE INFO

#### Article history:

Received 21 January 2013

Received in revised form 6 September 2013

Accepted 8 October 2013

Available online 28 October 2013

#### Keywords:

Cambrian Series 2 and Cambrian Series 3

Sulfide sulfur isotope

Degree of pyritization

Yangtze Platform

### ABSTRACT

The transition between Series 2 and Series 3 of the Cambrian Period was a time of environmental perturbations and biological innovations. A generally positive sulfur isotopic composition of sedimentary pyrite with  $\delta^{34}\text{S}_{\text{pyrite}}$  values between +1.7 and +37.3‰ is consistent with a biological origin via reduction of strongly  $^{34}\text{S}$  enriched seawater sulfate. No substantial changes in the redox conditions of the water column are discernible from the DOP record, and the sulfide sulfur isotopic composition is independent of DOP, in particular an excursion towards less  $^{34}\text{S}$  enriched values immediately preceding the proposed level of the Cambrian Series 2 to Cambrian Series 3 transition. This level is also characterized by a negative carbonate carbon isotope excursion, believed to reflect the transgressive flooding of the shelf with basinal anoxic waters. Low DOP values would suggest that these might have been ferruginous rather than sulfidic.

© 2013 Elsevier B.V. All rights reserved.

### 1. Introduction

The stratigraphic interval representing the Cambrian Series 2 and Cambrian Series 3 transition was a time of environmental perturbations and biological innovations (Sundberg et al., 1999; Zhao et al., 2001a,b; Guo et al., 2005; Zhao et al., 2008; Guo et al., 2010a; Sundberg et al., 2011). This transition is marked by a globally recognizable negative carbon isotope excursion (the ROECE event) that records the transgressive flooding of the shelf areas with  $^{13}\text{C}$  depleted basinal and previously anoxic bottom water. Respective changes have been archived in the sedimentary rocks from this time interval and are reflected, among others, in the temporal evolution of the carbon isotopic composition of carbonate and organic carbon in the Wuliu-Zengjiayan and Jianshan sections of southern China (e.g., Guo et al., 2010a).

This study aims at further reconstructing the environmental conditions by investigating temporal fluctuations in the sulfur isotopic composition of sedimentary pyrite ( $\delta^{34}\text{S}_{\text{pyrite}}$ ) and potential changes in redox conditions in these two sedimentary successions that were deposited on the Yangtze Platform, South China. As a side aspect, the global correlation potential of  $\delta^{34}\text{S}_{\text{pyrite}}$  for this transition will be evaluated.

In the modern marine realm, dissolved sulfate represents the most important sulfur compound. In fact, for the past 2.3 Ga, the input of sulfate into the oceanic reservoir resulted primarily from the riverine delivery of sulfate resulting from oxidative continental weathering with a

minor contribution from hydrothermal activity (e.g., Strauss, 2004; Reuschel et al., 2012; Strauss et al., 2013). The principal output functions of sulfate from the ocean into the rock record have been the precipitation of evaporitic sulfate (including the incorporation of sulfate into carbonates; cf. Takano, 1985; Calvert et al., 1996; Staudt et al., 1999; Strauss, 1999; Kampschulte et al., 2001; Lyons et al., 2003; Kampschulte and Strauss, 2004; Goldberg et al., 2007), and the process of bacterial sulfate reduction and the formation and subsequent burial of iron sulfide into marine sediments (e.g., Canfield, 2001). While the former process is not associated with any substantial sulfur isotope effect (e.g., Holser and Kaplan, 1966; Claypool et al., 1980), the biological sulfur cycling, most notably the microbial reduction of sulfate, is associated with a substantial fractionation of the sulfur isotopic composition, discriminating against the heavy  $^{34}\text{S}$  isotope and resulting in variable but generally negative  $\delta^{34}\text{S}$  values archived in the sedimentary pyrite (for a review, see e.g., Canfield, 2001, and Johnston, 2011). Frequently,  $\delta^{34}\text{S}$  values of biogenic pyrite vary between –40 and 20‰ (Clark and Fritz, 1997). Most recently, Sim et al. (2011) reported a large isotopic fractionation between oceanic sulfate and sedimentary sulfide of 66‰ for sulfate reducing bacteria, both from a natural setting as well as from laboratory culture. In general, the sulfur isotopic composition of sedimentary sulfur can be utilized to monitor perturbations of the global sulfur cycle (e.g., Strauss et al., 2013). But caution has to be exerted as the development of sulfate-limiting conditions in the water column and/or the pore water realm due to intense microbial sulfate reduction will result in the progressive enrichment of  $^{34}\text{S}$  yielding progressively more positive  $\delta^{34}\text{S}$  values.

\* Corresponding author. Tel./fax: +86 10 64889455.

E-mail address: [guoqj@igsnrr.ac.cn](mailto:guoqj@igsnrr.ac.cn) (Q. Guo).

In addition to the abundances and isotopic compositions of carbon and sulfur, iron abundances/speciation and related geochemical parameters such as the degree of pyritization (DOP; Raiswell et al., 1988) have been utilized for evaluating the geochemical conditions during pyrite formation within a given sedimentary environment. The DOP quantifies iron availability but has been related to the redox condition of the bottom water. Specifically, DOP values  $<0.45$  and  $>0.75$ , respectively, reflect deposition from an oxic or an anoxic to euxinic bottom water (Raiswell et al., 1988).

The present study examines the sulfur isotope geochemistry and DOP across the Cambrian Series 2 to Cambrian Series 3 transition in the Wuliu-Zengjiayan and Jianshan sections, Guizhou Province, South China.

## 2. Stratigraphy and sampling

A succession of carbonates and siliciclastic sediments spanning the Cambrian Series 2 to Cambrian Series 3 transition is exposed at the Wuliu-Zengjiayan section near Balang village (Taixiang County, Guizhou Province, South China; Fig. 1), and this section has been proposed as a potential Global Stratotype Section and Point (GSSP) for this boundary (Sundberg et al., 1999; Zhao et al., 2001a,b, 2007, 2008, 2012). Correlative strata are exposed in the Jianshan section which is located along a ridge of Jianshan Mountain, ca. 1.5 km west of Chuandong Village (Zhao et al., 2008) and ca. 8 km NE away from the Wuliu-Zengjiayan section. The Jianshan section represents an additional candidate section in support of the stratotype for the Cambrian Series 2 and Cambrian Series 3 transition (Zhao et al., 2008) (Fig. 1).

During Cambrian times, these sections were located in a low latitude position (Scotese and McKerrow, 1990; Saltzman et al., 2000). Both sections straddle the Cambrian Series 2 to Cambrian Series 3 transition. In terms of stratigraphic units, the studied sections comprise the upper part of the Qingxudong Formation, the Kaili Formation, and the lower

part of the Jialao Formation (Fig. 2). Lithologies include limestone, dolostone, and silty calcareous mudstone, with abundant fossils preserved in the Kaili Formation. Sediments of the Kaili Formation were deposited in a shelf environment presumably in a water depth between 90 and 300 m (Zhang et al., 1996).

The Kaili Formation at the Wuliu-Zengjiayan section is more than 200 m thick, and is composed of gray silty mudstone, calcareous mudstone and limestone (Zhao et al., 2001a,b; Guo et al., 2005; Zhao et al., 2007). Interbeds of marl are common in the lower and middle parts of the formation, containing abundant trilobite fossils, such as *Oryctocephalus*, *Bathynotus* and *Ovatoryctocara*. The FAD of *Oryctocephalus indicus* occurs at 52.8 m above the base of the Kaili Formation (Zhao et al., 2007; Guo et al., 2010a,b; Sundberg et al., 2011). The part of the Kaili Formation lying below this horizon belongs to the *Ovatoryctocara cf. granulata-Bathynotus keichouensis* assemblage zone (Zhao et al., 2012), and that above 52.8 m belongs to the *O. indicus* zone and *Peronopsis taijiangensis* zone (Zhao et al., 2012).

The Kaili Formation at the Jianshan section is also more than 200 m thick, and is composed of calcareous mudstone, silty mudstone and limestone (Zhao et al., 2008; Guo et al., 2010a). There are abundant trilobite fossils in Kaili Formation, such as *Oryctocephalus*, *Bathynotus*, *Peronopsis* and *Olenoides*. The FAD of *Oryctocephalus indicus* of the Cambrian Series, Stage 5 occurs at 44.25 m above the base of the Kaili Formation (Zhao et al., 2008). The portion of the Kaili Formation lying below this horizon belongs to the *Ovatoryctocara cf. granulata-Bathynotus keichouensis* assemblage zone, and that above 44.25 m belongs to the *O. indicus* zone and *Peronopsis taijiangensis* zone (Zhao et al., 2012).

According to a revised measurement of this section (Zhao et al., 2008, 2012), the transition from Cambrian Series 2 to Cambrian Series 3 is located at 52.8 m above the boundary between the Qingxudong and Kaili formations in the Wuliu-Zengjiayan section and at 44.25 m above the boundary between the Qingxudong and Kaili formations in

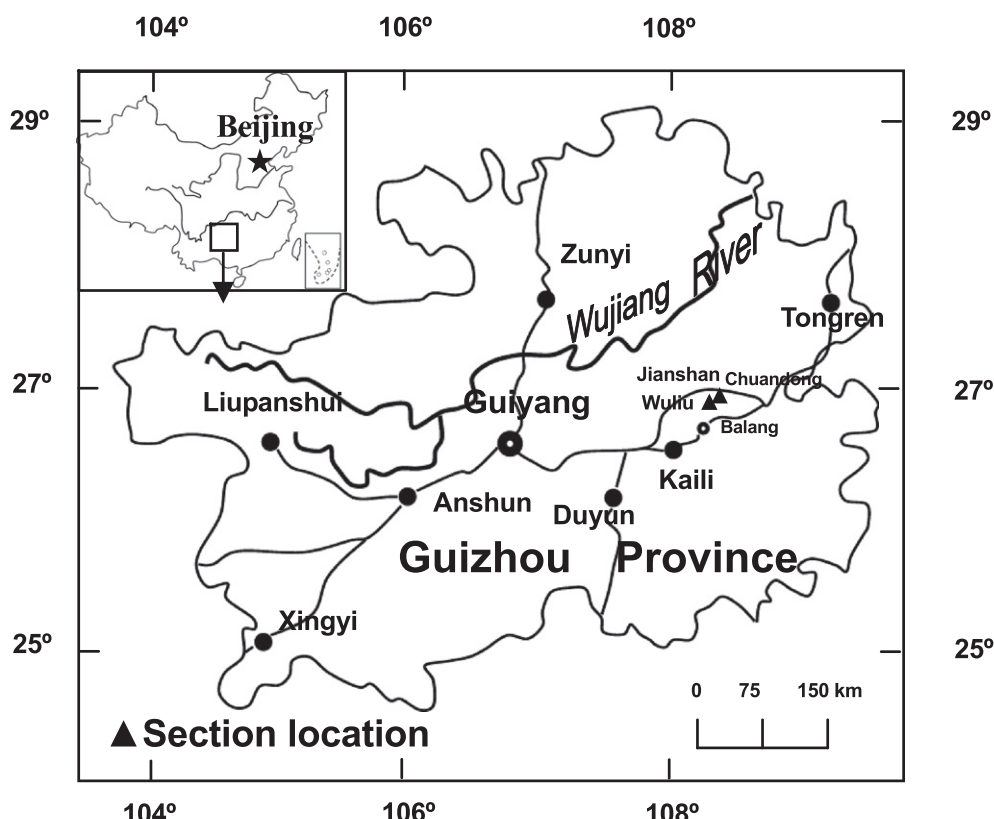


**Fig. 1.** Map showing the location of the Wuliu-Zengjiayan and Jianshan sections at Balang and Chuandong villages, Guizhou Province, South China.

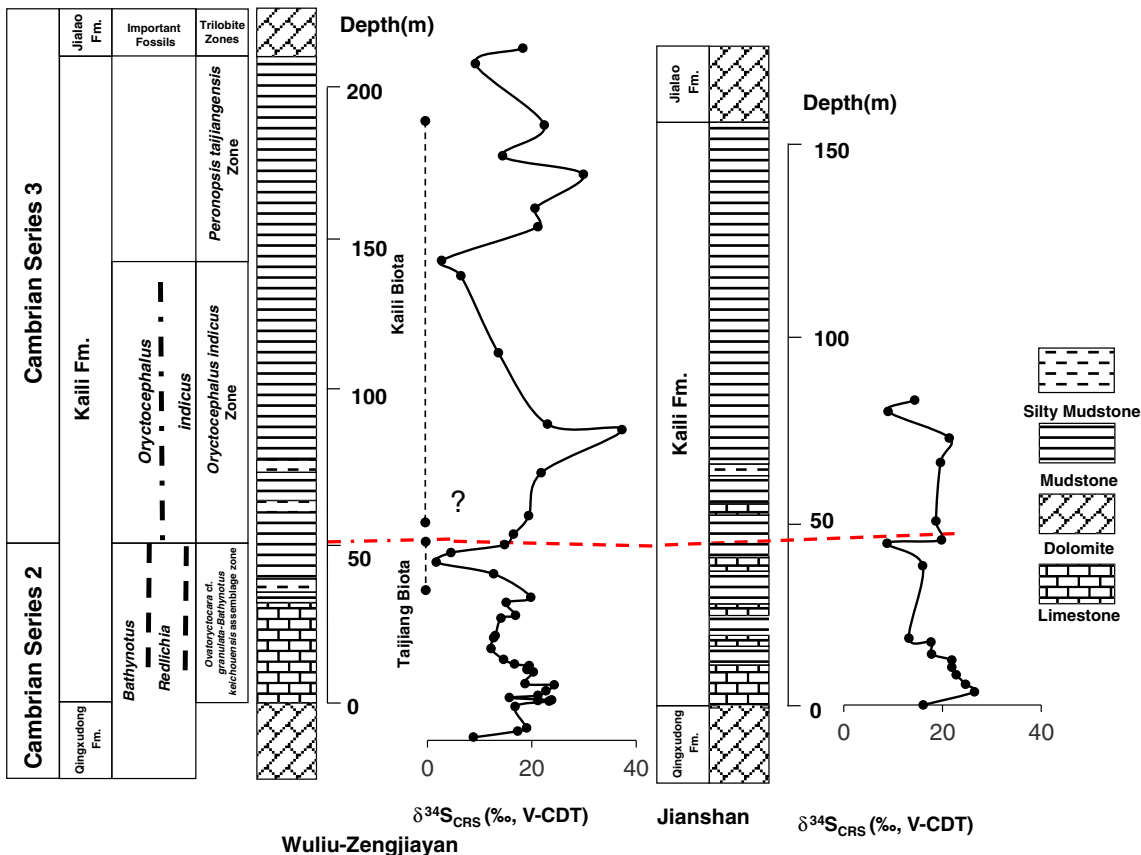


Fig. 2.  $\delta^{34}\text{S}_{\text{CRS}}$  profiles for the Wuliu-Zengjiayan and Jianshan sections.

the Jianshan section; here, we revise our measurements and data according to the above information (Table 1). The boundary is tentatively placed between the *Ovatoryctocara cf. granulata*–*Bathynotus keichouensis* assemblage zone and the *Oryctocephalus indicus* Zone in both sections (Zhao et al., 2007, 2008; Guo et al., 2010b; Zhao et al., 2012), and based on the first appearance data (FAD) of *O. indicus*. A transgressive event proposed for the transition from Cambrian Series 2 to Cambrian Series 3 resulted in changes in the depositional environment, with parts of the shelf being flooded by less oxygenated basinal bottom waters during the period (e.g., Montañez et al., 2000; Hough et al., 2006; Guo et al., 2010a). This was accompanied by a change in trilobite fauna (e.g., Zhao et al., 2008). A negative carbon isotope excursion occurs at the level of the Cambrian Series 2 to Cambrian Series 3 transition and it is believed to record a perturbation of the global carbon cycle associated with this transgressive flooding event (e.g., Guo et al., 2010a).

### 3. Analytical methods

Forty-four samples from the Wuliu-Zengjiayan section were analyzed and 17 samples from the Jianshan section (Guo et al., 2005, 2010a). Samples were dried at room temperature and pulverized in an agate mortar. Total sulfur (TS) and total carbon (TC) abundances were measured using IR spectroscopy following the liberation of carbon dioxide and sulfur dioxide from rock powders via combustion in an oxygen stream at 1350 °C. Total inorganic carbon (TIC) was liberated through acid-digestion and determined via IR spectroscopy of the resulting carbon dioxide. The content of total organic carbon (TOC) was determined as difference between TC and TIC. Analyses were performed using a CS-MAT 5500 at the Institut für Geologie und Paläontologie in Münster, Germany. The detection limit for these measurements was 0.1 wt.%

Different sulfur species (acid volatile sulfide (AVS), i.e. monosulfides, chromium reducible sulfur (CRS), consisting primarily of pyrite sulfur,

and organically bound sulfur (OBS), reflecting largely kerogen-bound sulfur) were extracted from the sediment samples for sulfur isotope analyses through a sequential wet chemical analysis (Canfield et al., 1986). Briefly, AVS was liberated with HCl (25%) and CRS with 1 M chromous chloride solution, both times under reducing conditions (flow of nitrogen). Resulting hydrogen sulfide was trapped as zinc sulfide using a zinc acetate trapping solution (3%) and subsequently converted to silver sulfide with 0.1 M silver nitrate. The remaining rock powder was treated with Eschka reagent at 800 °C (ASTM, 1977), liberating the remaining organic sulfur as water soluble sulfate. This was precipitated as barium sulfate using 8.5% BaCl<sub>2</sub>-solution.

Barium sulfate and silver sulfide precipitates from the different forms of sedimentary sulfur were measured for their  $\delta^{34}\text{S}$  values via isotope ratio mass spectrometry using a ThermoFinnigan Delta Plus mass spectrometer interfaced with an elemental analyzer (EA-IRMS) in Münster, Germany. Results are reported in the usual delta notation as per mil difference to the Vienna Canyon Diablo Standard (V-CDT). Reproducibility as determined from replicate measurements of samples and standard materials was better than  $\pm 0.3\text{\%}$ .

HCl-soluble iron ( $\text{Fe}_{\text{HCl}}$ ) was extracted from the bulk sediment with cold 1 M HCl for 24 h and the Fe concentration was subsequently measured by inductively coupled plasma optical emission spectroscopy (ICP-OES) in Münster, Germany. Pyrite-bound iron ( $\text{Fe}_{\text{pyr}}$ ) was calculated based on pyrite sulfur abundances. The sum of both Fe species reflects Fe that is reactive towards hydrogen sulfide. DOP was calculated as:  $\text{DOP} = \text{Fe}_{\text{pyr}} / (\text{Fe}_{\text{HCl}} + \text{Fe}_{\text{pyr}})$ .

### 4. Results

Analytical results are presented in Tables 1 and 2. TS abundances are quite variable, yet generally below 0.1 wt.% for both localities. Samples range around an average TS value of  $0.09 \pm 0.15\text{ wt.\%}$  ( $n = 61$ ) but

**Table 1**

Analytical results for samples from the Wuliu-Zengjiayan section, Guizhou Province, South China.

Sample	Unit name	Lithology	Depth (m) (revised)	$\delta^{34}\text{CRS}$ (‰, V-CDT)	$\delta^{13}\text{C}_{\text{carb}}$ (‰, V-PDB)	Sample weight (g)	Ag <sub>2</sub> S- CRS (g)	Ag <sub>2</sub> S (mol)	Fe <sub>pyr</sub> (mol)	FeS <sub>2</sub> (g)	Fe <sub>pyr</sub> (wt. %)	Fe <sub>HCl</sub> (wt. %)	Fe <sub>HCl</sub> (ppm)	DOP	TC	TIC	TOC	TS		
																			(wt. %)	
1	Qingxudong Fm.	Dolomite	−11.6	8.8	0.8	5.24	0.089	0.00036	0.00018	0.01005	0.192	0.002	24.22	0.99	10.38	10.11	0.28	0.10		
3	Qingxudong Fm.	Dolomite	−9.6	17.3	2.1	6.4	0.077	0.00031	0.00016	0.00868	0.136	0.010	102.35	0.93	10.4	9.47	0.92	0.01		
4	Qingxudong Fm.	Limestone	−8.6	19	2.2	5.25	0.151	0.00061	0.00031	0.01709	0.326	0.008	78.26	0.98	8.69	7.96	0.74	0.10		
5	Qingxudong Fm.	Dolomite	−1.6	16.8	−0.3	5.73	0.049	0.00020	0.00010	0.00550	0.096	0.080	802.49	0.54	12.61	12.35	0.26	0.00		
8	Kaili Fm.	Limestone	0.1	23.3	2.4	8.2	0.171	0.00069	0.00034	0.01927	0.235	0.012	117.54	0.95	9.33	8.81	0.52	0.11		
9	Kaili Fm.	Limestone	0.3	21.2	2.5	0.61	0.034	0.00014	0.00007	0.00379	0.621	0.183	1829.90	0.77	10.2	9.77	0.43	0.09		
10	Kaili Fm.	Limestone	0.5	23.8	2.7	3.9	0.002	0.00001	0.00000	0.00021	0.006	0.030	299.59	0.16	9.03	8.83	0.2	0.00		
11	Kaili Fm.	Limestone	1.3	15.7	2.7	10.2	0.004	0.00002	0.00001	0.00046	0.005	0.025	245.47	0.16	8.82	8.4	0.42	0.00		
12	Kaili Fm.	Limestone	2	21.2	2	1.31	0.043	0.00017	0.00009	0.00483	0.369	0.047	468.86	0.89	8.41	7.8	0.61	0.10		
14	Kaili Fm.	Limestone	3.5	22.7	2.4	1.85	0.013	0.00005	0.00003	0.00152	0.082	0.033	331.74	0.71	7.21	6.8	0.41	0.00		
15	Kaili Fm.	Muddy limestone	5.4	24.3	2.3	4.02	0.018	0.00007	0.00004	0.00204	0.051	0.577	5770.38	0.08	4.32	3.86	0.46	0.01		
17	Kaili Fm.	Limestone	5.8	18.7	2.4	5.09	0.161	0.00065	0.00032	0.01814	0.356	0.087	865.46	0.80	8.68	8.13	0.56	0.16		
21	Kaili Fm.	Muddy limestone	9.6	20.3	2.4	1.1	0.039	0.00016	0.00008	0.00441	0.416	0.583	5825.00	0.42	8.39	7.91	0.48	0.21		
22	Kaili Fm.	Muddy limestone	10.4	19.1	2.4	1.8	0.039	0.00016	0.00008	0.00441	0.244	0.082	821.36	0.75	9.68	9.38	0.3	0.31		
23	Kaili Fm.	Limestone	11	19.2	2.3	2.5	0.042	0.00017	0.00008	0.00474	0.190	0.023	226.21	0.89	10.33	9.53	0.81	0.01		
24	Kaili Fm.	Calcareous mudstone	11.7	19.5	1.9	2.79	0.048	0.00019	0.00010	0.00541	0.194	0.008	78.29	0.96	1.61	1.09	0.53	0.15		
25	Kaili Fm.	Muddy limestone	12.2	16.7	1.4	8.22	0.165	0.00067	0.00033	0.01868	0.227	0.035	352.92	0.87	7.71	7.35	0.35	0.06		
27	Kaili Fm.	Muddy limestone	13.7	14.6	0.9	1.73	0.013	0.00005	0.00003	0.00148	0.086	0.023	230.47	0.79	8.26	7.66	0.6	0.00		
31	Kaili Fm.	Silty limestone	17.2	12.2	0.6	11.85	0.031	0.00012	0.00006	0.00348	0.029	0.116	1159.10	0.20	7.49	7.49	0	0.00		
35	Kaili Fm.	Silty mudstone	20.7	12.7	0.6	13.36	0.056	0.00023	0.00011	0.00631	0.047	0.095	951.67	0.33	8.32	8.07	0.26	0.02		
36	Kaili Fm.	Silty limestone	21.4	13	0.9	6.5	0.014	0.00006	0.00003	0.00162	0.025	0.054	543.83	0.31	7.6	7.35	0.25	0.00		
43	Kaili Fm.	Silty limestone	27.1	14.1	0.4	10.85	0.003	0.00001	0.00001	0.00033	0.003	0.085	8854.72	0.00	7.17	6.98	0.19	0.01		
45	Kaili Fm.	Silty mudstone	28	16.9	0.3	13.23	0.003	0.00001	0.00001	0.00035	0.003	1.110	11,098.00	0.00	1.2	1.09	0.21	0.01		
49	Kaili Fm.	Mudstone	32.2	15.1	−1.2	13.54	0.001	0.00000	0.00000	0.00006	0.000	3.018	30,175.04	0.00	1.191	0.82	0.37	0.01		
49-1	Kaili Fm.	Mudstone	33.9	19.8	15	0.009	0.00004	0.00002	0.00104	0.007	0.989	9885.00	0.01	4.5	4.38	0.12	0.00			
55-1	Kaili Fm.	Mudstone	41.5	12.7	2.3	0.048	0.00019	0.00010	0.00540	0.108	1.243	12,428.76	0.16	0.53	0.47	0.06	0.00			
61-1	Kaili Fm.	Muddy carbonate	45.3	1.7	20	0.015	0.00006	0.00003	0.00170	0.009	2.231	22,307.00	0.00	0.28	0.2	0.08	0.00			
66-1	Kaili Fm.	Mudstone	48.4	4.5	3.06	0.013	0.00005	0.00003	0.00145	0.007	2.408	24,076.00	0.00	0.32	0.27	0.05	0.00			
78	Kaili Fm.	Mudstone	51	14.8	−1.3	14.05	0.001	0.00000	0.00000	0.00008	0.001	3.714	37,139.18	0.00	0.43	0.1	0.33	0.01		
91-1	Kaili Fm.	Mudstone	54.4	16.5	2.26	0.000	0.00000	0.00000	0.00005	0.002	1.475	14,749.00	0.13	0.86	0.75	0.11	0.01			
93-1	Kaili Fm.	Mudstone	60.4	19.4	10	0.000	0.00000	0.00000	0.00005	0.001	1.888	18,879.35	0.00	1.34	1.21	0.12	0.00			
98-1	Kaili Fm.	Muddy limestone	74.4	21.8	10	0.001	0.00000	0.00000	0.00009	0.001	3.092	30,920.80	0.00	0.24	0.16	0.08	0.00			
99	Kaili Fm.	Limestone	88.4	37.3	0.1	3.46	0.140	0.00057	0.00028	0.01583	0.458	0.005	48.74	0.99	5.7	5.46	0.23	0.44		
100	Kaili Fm.	Limestone	90.2	23	0.1	14.15	0.085	0.00034	0.00017	0.00956	0.068	0.031	310.10	0.69	5.39	4.56	0.83	0.01		
102	Kaili Fm.	Muddy carbonate	113.4	13.6	−0.1	14.24	0.003	0.00001	0.00001	0.00038	0.003	0.060	597.00	0.52	4.77	4.52	0.25	0.00		
105	Kaili Fm.	Dolomite	138.4	6.4	−0.2	5.5	0.014	0.00006	0.00003	0.00155	0.028	0.102	1023.00	0.42	11.22	11.25	0.04	0.01		
106	Kaili Fm.	Limestone	143.4	2.7	−1.1	10.41	0.079	0.00032	0.00016	0.00892	0.086	0.136	1356.21	0.39	7.16	6.93	0.24	0.03		
108	Kaili Fm.	Limestone	154.4	21.2	0.1	10.03	0.057	0.00023	0.00012	0.00649	0.065	0.194	1944.87	0.25	4.7	4.61	0.09	0.04		
109	Kaili Fm.	Calcareous mudstone	160.4	20.6	0.5	5.17	0.076	0.00031	0.00015	0.00858	0.166	4.616	46,160.23	0.03	3.06	2.71	0.35	0.23		
110	Kaili Fm.	Limestone	171.4	29.9	0.1	9.61	0.003	0.00001	0.00001	0.00033	0.003	0.002	24.48	0.58	10.16	10.04	0.12	0.02		
111	Kaili Fm.	Calcareous mudstone	177.4	14.4	−0.5	1.53	0.078	0.00031	0.00016	0.00880	0.575	2.093	20,930.48	0.22	2.93	2.44	0.49	0.67		
112	Kaili Fm.	Limestone	187.4	22.4	0.8	12.75	0.059	0.00024	0.00012	0.00670	0.053	0.002	24.48	0.96	10.84	10.85	0.01	0.01		
113	Kaili Fm.	Limestone	207.4	9.2	0.8	7.2	0.084	0.00034	0.00017	0.00950	1.319	0.258	2578.00	0.34	11.71	11.25	0.46	0.00		
114	Jialao Fm.	Dolomite	212.4	18.3	2	6.17	0.123	0.00050	0.00025	0.01393	0.226	0.015	152.10	0.94	10.07	9.15	0.93	0.01		

include a maximum value of 0.67 wt.%. Total carbon (TC) abundances vary between 0.24 and 12.61 wt.% around an average value of  $6.7 \pm 3.7$  wt.% (n = 61). Total inorganic carbon (TIC) abundances vary between 0.1 and 12.35 wt.% around an average value of  $6.35 \pm 3.6$  wt.% (n = 61). Total organic carbon (TOC) abundances vary between 0.001 and 0.93 wt.% around an average value of  $0.35 \pm 0.23$  wt.% (n = 61).

None of the samples yielded any acid-volatile sulfide during the sequential wet chemical extraction. Highly variable, yet all positive pyrite sulfur isotope values ( $\delta^{34}\text{S}_{\text{CRS}}$ ) between 1.7 and 37.3‰ characterize sediments from the Wuliu-Zengjiayan section (average value of  $17.2 \pm 6.7$ ‰,

n = 44). Sediments from the Jianshan section display a pyrite sulfur isotopic composition between 8.8 and 26.5‰ (average value of  $18.3 \pm 5$ ‰, n = 17). Only three samples from the Jianshan section yielded sufficient OBS for a sulfur isotope measurement.  $\delta^{34}\text{S}_{\text{OBS}}$  values vary between 14.1 and 23.2‰ and are, thus, within the range of sulfur isotope values measured for chromium reducible sulfur (Tables 1 and 2).

Fe abundances are extremely variable and calculated DOP results are equally variable ranging from <0.1 to 0.99 (n = 41) for samples from the Wuliu-Zengjiayan section and between <0.1 and 0.99 (n = 17) for samples from the Jianshan section (Tables 1 and 2).

**Table 2**

Analytical results for samples from the Jianshan section, Guizhou Province, South China.

Sample	Unit name	Depth (m) (revised)	Lithology	$\delta^{34}\text{Scrs}$ (‰, V-CDT)	$\delta^{34}\text{SOBS}$ (‰, V-PDB)	$\delta^{13}\text{Ccarb}$ (‰, V-PDB)	Sample weight (g)	Ag <sub>2</sub> S CRS (g)	Ag <sub>2</sub> S (mol)	Fe <sub>pyr</sub> (mol)	Fe <sub>S2</sub> (g)	Fe <sub>pyr</sub> (wt. %)	Fe <sub>HCl</sub> (wt. %)	Fe <sub>HCl</sub> (ppm)	DOP	TC	TIC	TOC	TS
CD501	Kaili Fm.	0	Limestone	16.1		-0.3	12	0.020	0.00008	0.00004	0.00230	0.019	0.032	322.45	0.37	11.99	11.78	0.21	0.02
CD504	Kaili Fm.	3.5	Limestone	26.5		2.8	2.03	0.102	0.00041	0.00021	0.01156	0.570	0.002	24.93	1.00	9.47	9.31	0.15	0.32
CD505	Kaili Fm.	5.5	Limestone	24.7		2.1	4.2	0.139	0.00056	0.00028	0.01568	0.373	0.013	130.10	0.97	8.65	8.05	0.61	0.13
CD506	Kaili Fm.	8	Limestone	22.8	23.2	2	2.4	0.070	0.00028	0.00014	0.00785	0.327	0.010	104.26	0.97	8.88	8.53	0.35	0.29
CD507	Kaili Fm.	10	Limestone	21.9		2.3	6.13	0.125	0.00050	0.00025	0.01406	0.229	0.027	5266.55	0.30	8.58	8.12	0.46	0.08
CD508	Kaili Fm.	11.9	Limestone	21.9	18.3	2.3	3.24	0.054	0.00022	0.00011	0.00611	0.188	0.462	4620.78	0.29	8.91	8.38	0.53	0.22
CD509	Kaili Fm.	13.5	Limestone	17.8		3.1	7.25	0.133	0.00054	0.00027	0.01499	0.207	0.003	25.11	0.99	10.19	9.71	0.48	0.05
CD511	Kaili Fm.	16.7	Limestone	17.7	14.1	0.6	7.45	0.124	0.00050	0.00025	0.01399	0.188	0.005	49.81	0.97	7.95	7.55	0.4	0.10
CD512	Kaili Fm.	17.7	Limestone	13.2		1.2	50	0.006	0.00003	0.00001	0.00072	0.001	0.602	6015.50	0.00	8.12	7.72	0.4	0.00
CD527	Kaili Fm.	36.9	Limestone	16		0	10	0.013	0.00005	0.00003	0.00147	0.015	0.942	9423.00	0.02	8.32	8.01	0.31	0.00
CD531	Kaili Fm.	42.8	Calcareous mudstone	8.8		-2.1	0.79	0.042	0.00017	0.00009	0.00479	0.606	2.168	21,675.00	0.22	1.63	1.14	0.5	0.65
CD513	Kaili Fm.	43.7	Limestone	19.8		-6.8	13	0.098	0.00040	0.00020	0.01110	0.085	0.343	3433.90	0.20	9.74	9.76	0	0.01
CD534	Kaili Fm.	48.7	Calcareous mudstone	18.7		-2.6	4.5	0.115	0.00046	0.00023	0.01298	0.289	0.867	8670.00	0.25	0.6	0.42	0.18	0.00
CD537	Kaili Fm.	64.2	Muddy limestone	19.6		-2.3	4.26	0.149	0.00060	0.00030	0.01684	0.395	0.569	5690.00	0.41	1.47	1.09	0.38	0.01
CD514	Kaili Fm.	70.7	Limestone	21.4		-0.7	10	0.015	0.00006	0.00003	0.00164	0.016	0.783	7827.00	0.02	7.94	7.6	0.34	0.00
CD516	Kaili Fm.	77.7	Muddy limestone	9		-0.6	3.47	0.117	0.00047	0.00024	0.01319	0.380	0.617	6168.67	0.38	4.44	3.88	0.56	0.40
CD519	Kaili Fm.	80.7	Limestone	14.4		-0.4	4.75	0.076	0.00030	0.00015	0.00854	0.180	0.513	5133.00	0.26	8.39	8.3	0.09	0.09

## 5. Discussion

The temporal evolution of the global sulfur cycle has been successfully reconstructed by utilizing the sulfur isotopic composition of ancient seawater sulfate from evaporitic sulfate minerals (e.g., Claypool et al., 1980) or trace quantities of sulfate incorporated into carbonate,

termed structurally substituted sulfate (SSS) or carbonate-associated sulfate (CAS) (e.g., Kampschulte and Strauss, 2004; Gill et al., 2007; Wothe et al., 2012). The sulfate sulfur isotopic record is characterized by oscillations on different time scales, reflecting perturbations of the global sulfur cycle (e.g., Strauss, 2004). The late Neoproterozoic and early Paleozoic are characterized by  $\delta^{34}\text{S}$  values generally more positive

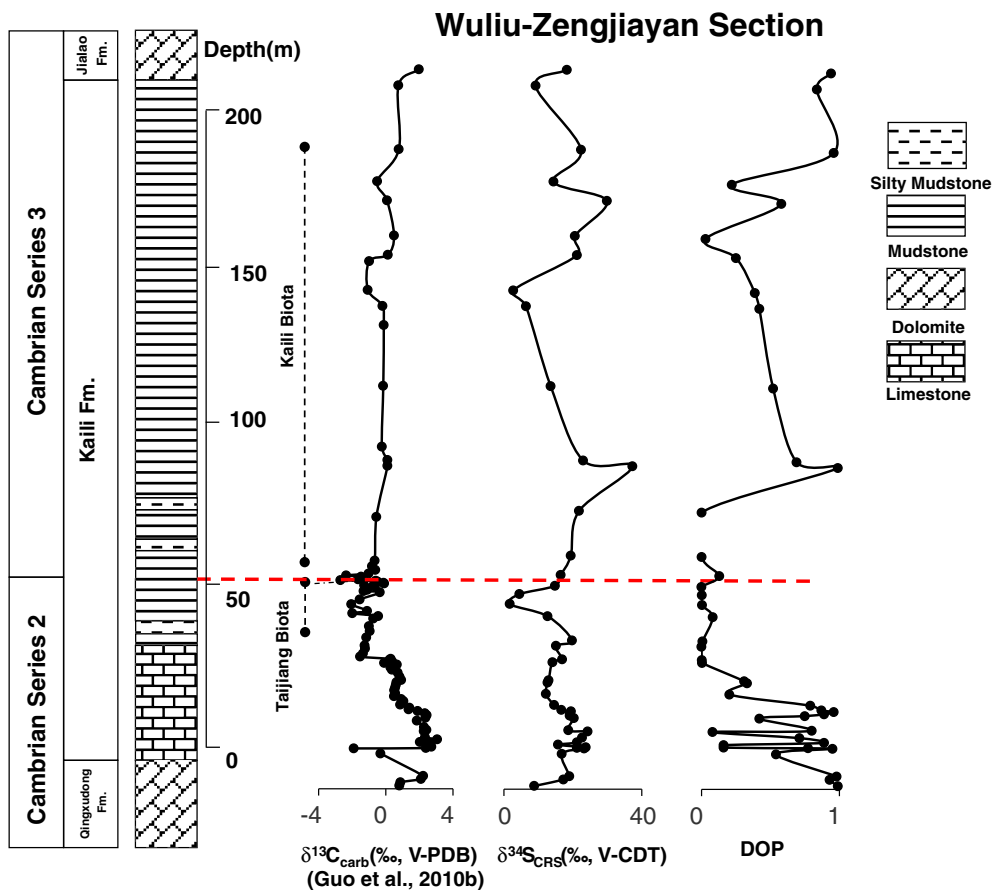
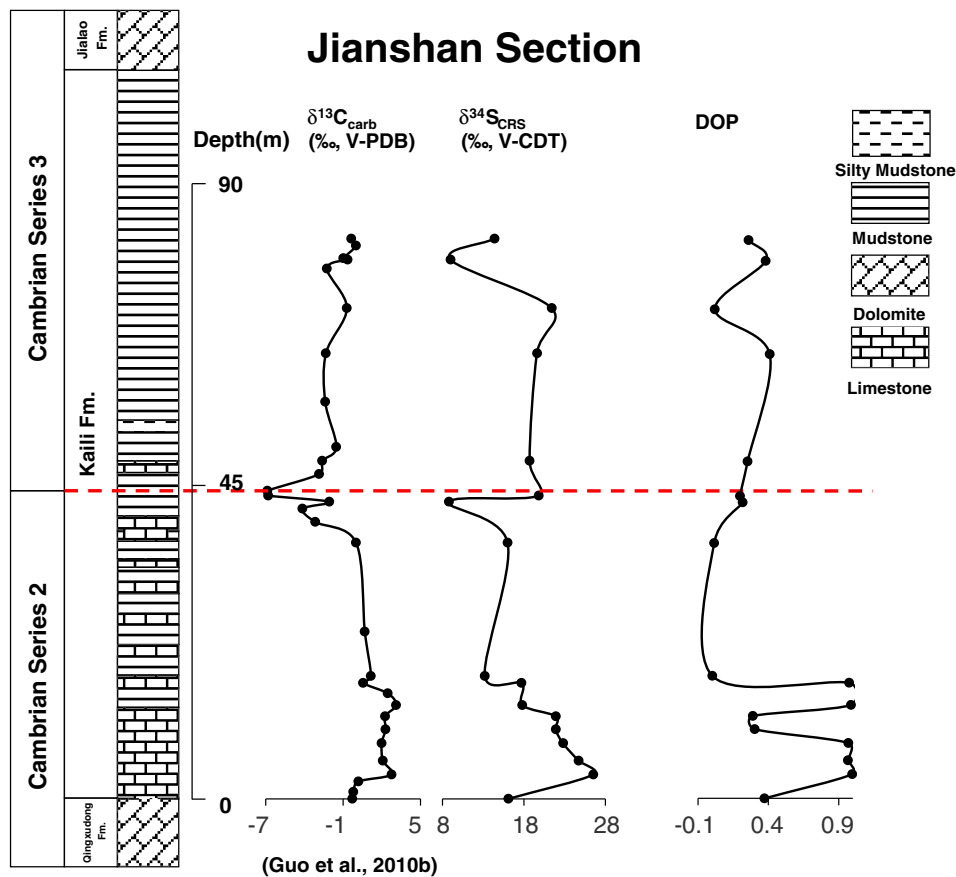


Fig. 3.  $\delta^{34}\text{S}_{\text{CRS}}$ ,  $\delta^{13}\text{C}_{\text{carb}}$ , DOP profiles for the Wuliuzengjiayan, Guizhou Province, South China.



**Fig. 4.**  $\delta^{34}\text{S}_{\text{CRS}}$ ,  $\delta^{13}\text{C}_{\text{carb}}$ , DOP profiles for the Jianshan sections, Guizhou Province, South China.

than +30‰ (e.g., Claypool et al., 1980; Shields et al., 1999, 2004; Kampschulte and Strauss, 2004; Goldberg et al., 2005; Halverson and Hurtgen, 2007; Fike and Grotzinger, 2008; Kaufman et al., 2009; Wotte et al., 2011, 2012; Loyd et al., 2012) including strongly  $^{34}\text{S}$  enriched values of more than +50‰ for traditional middle Cambrian strata in Siberia (Kouchinsky et al., 2008; Wotte et al., 2011) and Australia (Hough et al., 2006). Based on an isotope mass balance, the overall  $^{34}\text{S}$  enriched sulfate sulfur isotope signature reflects the enhanced deposition of  $^{34}\text{S}$  depleted sulfide sulfur. Respective perturbations of the seawater sulfate sulfur isotopic composition could be related to sea level oscillations resulting in the expansion/reduction of areas in which bacterial sulfate reduction prevailed (e.g., Wotte et al., 2012). In addition to the perturbations of the global sulfur cycle, variations in sulfate sulfur isotope signatures reflecting spatial/temporal variations on the regional scale can be superimposed on the global sulfur isotope record (cf., Guo et al., 2009).

In general, the sulfur isotopic composition of sedimentary pyrite broadly parallels the marine sulfate sulfur isotope record (e.g., Canfield, 2001), yet with substantial larger variability. The latter is caused by differences in sulfur isotopic fractionation associated with bacterial sulfate reduction under different environmental conditions. Most importantly, the magnitude in sulfur isotope fractionation is dependent on the sulfate concentration. It is generally accepted that the Cambrian seawater is characterized by a low sulfate concentration of ca. 5–12 mM (cf., Brennan et al., 2004; Hough et al., 2006; Gill et al., 2007; Hurtgen et al., 2009; Gaines et al., 2012). Although a substantial decrease in sulfur isotopic fractionation appears to be limited to very low sulfate concentrations (<200  $\mu\text{M}$ ; cf. Habicht et al., 1998), an overall low oceanic sulfate concentration during Cambrian times is prone to the development of sulfate limitation with resulting heterogeneities in the sulfur isotopic composition of sedimentary sulfur (Hurtgen et al., 2006; Ries et al., 2009).

Consequently, the evolution towards more positive  $\delta^{34}\text{S}$  values could reflect the development of closed system conditions in the early burial environment with respect to sulfate availability in the pore water realm (e.g., Canfield, 2001).

##### 5.1. Wuliu-Zengjiayan section

The present study aims at investigating whether the proposed perturbations of the global carbon cycle across the Cambrian Series 2 to Cambrian Series 3 transition archived in the sedimentary successions in Guizhou, South China (Guo et al., 2010a) are accompanied by respective changes in the global sulfur cycle. For this, the sulfur isotopic composition of sedimentary pyrite has been studied which indeed displays substantial variations across the stratigraphic succession exposed in the Wuliu-Zengjiayan section (black line in Fig. 3). The observed range in  $\delta^{34}\text{S}_{\text{CRS}}$  is consistent with a biological origin and an isotopic fractionation associated with bacterial sulfate reduction, despite the fact that the sulfur isotopic composition of the Cambrian seawater sulfate reservoir is poorly constrained and was likely heterogeneous (e.g., Hurtgen et al., 2009; Gill et al., 2011; Wotte et al., 2012). An excursion towards less  $^{34}\text{S}$  enriched values is located slightly below the level of the Cambrian Series 2 to Cambrian Series 3 transition.

In order to identify potential causes for the observed stratigraphic variations in  $\delta^{34}\text{S}$  and to further evaluate the correlation potential of these sulfur isotope excursions, additional geochemical parameters can be considered. As a first observation, no clear correlations are discernible between the  $\delta^{34}\text{S}_{\text{CRS}}$  and TC, TIC, TOC, TS and DOP (Fig. 5A). We will carefully examine this observation trying to answer the most obvious question: does the stratigraphic variation in  $\delta^{34}\text{S}_{\text{CRS}}$  reflect a perturbation of the global sulfur cycle or are the observed isotope excursions reflecting changes in the environmental conditions in the pore

water realm during progressive diagenesis. The latter in particular would render any stratigraphic correlation questionable.

In respect to reconstructing biogeochemical processes in marine sediments, a number of different parameters can be considered. The degree of pyritization has been developed in order to quantify iron availability during the process of sulfide formation associated with bacterial sulfate reduction. Empirical evidence from fine grained siliciclastic sediments suggested that iron availability was further related to the redox conditions within the depositional environment and that the DOP could be used as a proxy signal for characterizing the redox state of the bottom water (e.g., Raiswell et al., 1988). This was an important observation as it provides information about whether bacterial sulfate reduction and subsequent pyrite formation could have occurred within the anoxic bottom water column or whether it happened in the pore water realm during sediment diagenesis. With respect to the sulfur isotopic composition, a high DOP and, thus, iron-limiting conditions, could indicate that only part of the sulfur isotope signature has been archived (Fig. 3).

DOP values vary widely across stratigraphy of the Wuliu-Zengjiayan section (Fig. 3). Closer inspection, however, reveals a correlation between DOP and lithology. This is most clearly expressed in the lower part of the section where the carbonates of the lower Kaili Formation display high DOP values whereas the overlying mudstone shows low DOP values. Higher up in stratigraphy, the picture becomes less clear

with moderate to high DOP values in the mudstones and siltstones above the Cambrian Series 2 to Cambrian Series 3 transition. Most conspicuous is a DOP value of 0.99 at a depth of 88.4 m, defining a single-point-excursion. This high DOP value characterizes a sample with a moderate TIC value of 5.6 wt.%, a very low concentration of  $\text{Fe}_{\text{HCl}}$  (48.7 ppm) and the most positive  $\delta^{34}\text{S}_{\text{CRS}}$  value of +37.3‰. Overall, only few samples show DOP values above the threshold of 0.75 for reflecting anoxic bottom water conditions. All of them are lithologically described as limestones, located in the lower or uppermost part of the Kaili Formation. Most importantly, however, the transition from Cambrian Series 2 to Cambrian Series 3, located in the Wuliu-Zengjiayan section at a depth of 52.8 m above the base of the Kaili Formation, is not associated with a change in the redox conditions.

Looking at the relationship between DOP and  $\delta^{34}\text{S}_{\text{CRS}}$ , no obvious correlation is discernible (Fig. 5A). Most  $\delta^{34}\text{S}_{\text{CRS}}$  values lie between +12 and +25‰ independent of their DOP values. Even the more  $^{34}\text{S}$  depleted values don't show a clear dependency towards DOP. Solely the most  $^{34}\text{S}$  enriched  $\delta^{34}\text{S}_{\text{CRS}}$  value of +37.3‰ is characterized by a high DOP value of 0.99, but this could well be a consequence of a generally low Fe abundance of this carbonate rock.

In summary, sediments of the Wuliu-Zengjiayan section display large variations in  $\delta^{34}\text{S}_{\text{CRS}}$ . These appear to be independent of lithology and redox-state of the depositional environment.

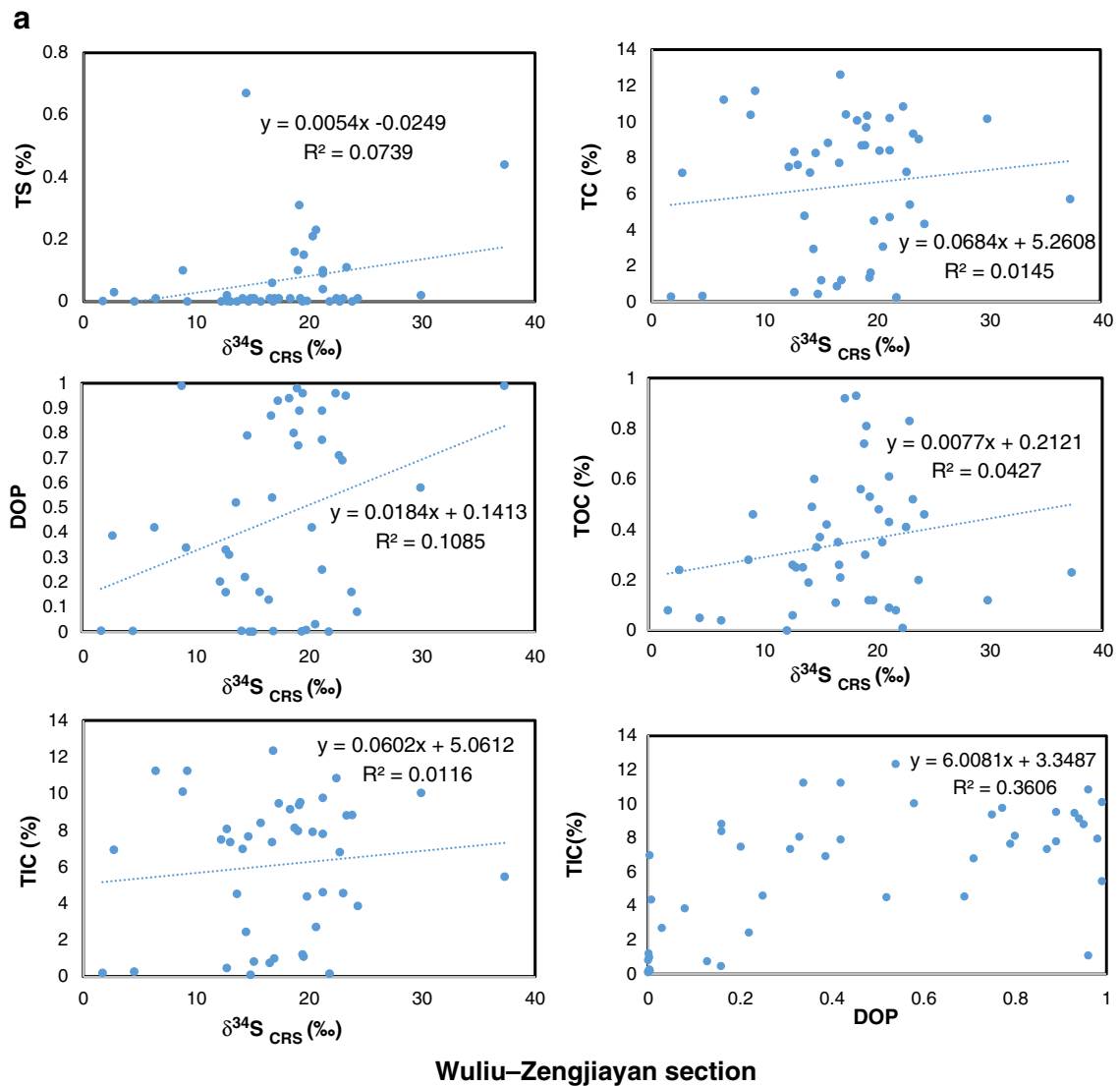


Fig. 5. Cross-plot of  $\delta^{34}\text{S}_{\text{CRS}}$  and TC,  $\delta^{34}\text{S}_{\text{CRS}}$  and TIC,  $\delta^{34}\text{S}_{\text{CRS}}$  and TOC,  $\delta^{34}\text{S}_{\text{CRS}}$  and TS,  $\delta^{34}\text{S}_{\text{CRS}}$  and DOP, DOP and TS for the Wuliu-Zengjiayan (a) and Jianshan (b) sections.

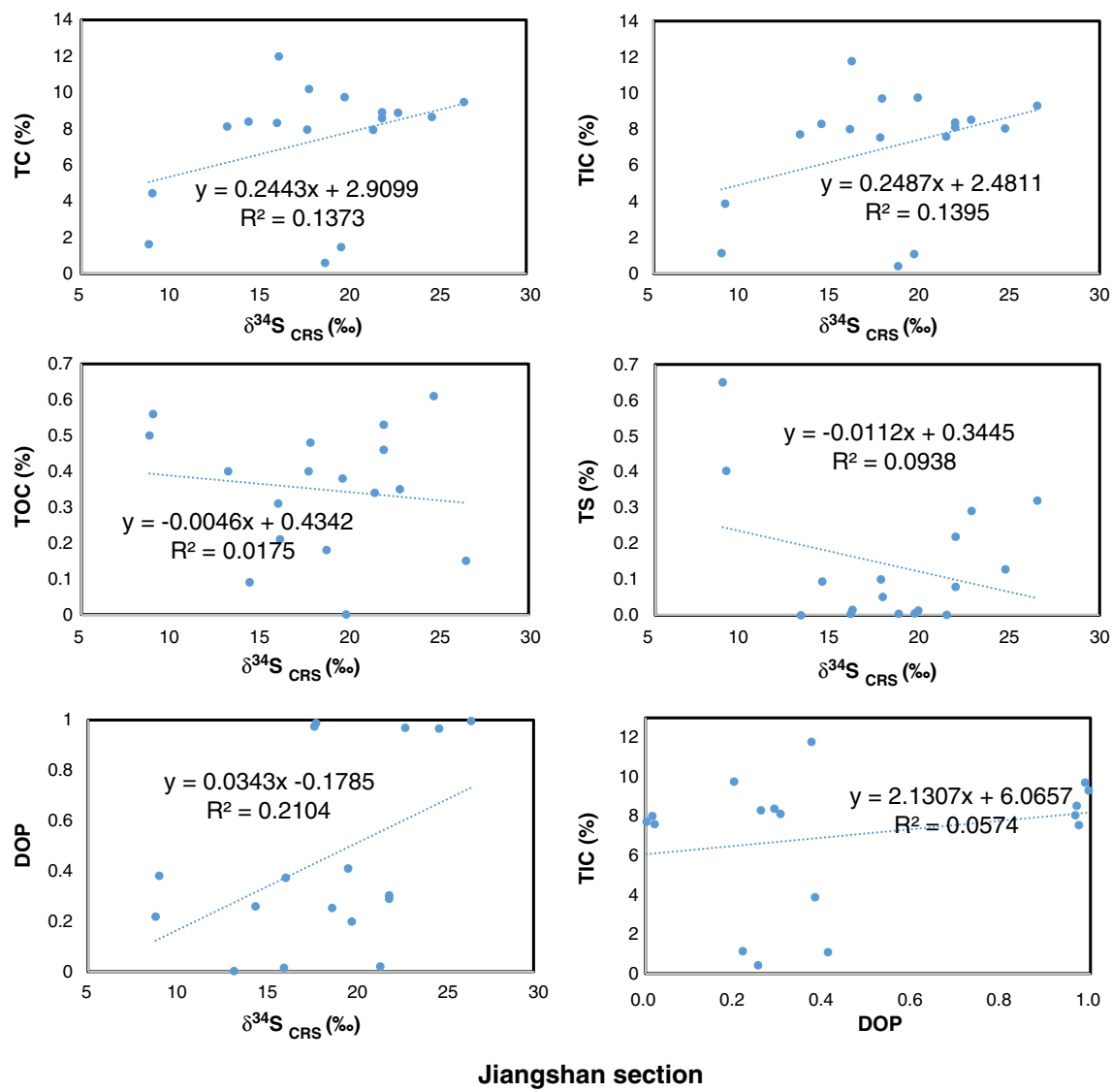


Fig. 5 (continued).

### 5.2. Jianshan section

The pyrite sulfur isotopic composition ( $\delta^{34}\text{S}_{\text{CRS}}$ ) displays sizeable variations across the stratigraphic succession exposed in the Jianshan section (Fig. 4). They are interpreted to result from bacterial sulfate reduction and subsequent pyrite formation. Again, the pyrite sulfur isotope values appear independent of the host lithology. Similarly to the Wuliu-Zengjiayan section, no clear correlation is discernible between  $\delta^{34}\text{S}_{\text{CRS}}$  and the abundances of carbon and sulfur as well as with the DOP (Fig. 5B). DOP values display substantial variations between <0.1 and 0.99. However, all samples that are characterized by a DOP above the threshold for anoxic bottom water conditions are located in the lower part of the Kaili Formation and are limestone samples. The proposed Cambrian Series 2 to Cambrian Series 3 transition at a stratigraphic level of 44.25 m above the base of the Kaili Formation is also not associated with a change in the prevailing redox conditions.

### 5.3. Palaeoenvironmental considerations

Two important observations have been made for both sedimentary sections studied. Sediments across the immediate transition from Cambrian Series 2 to Cambrian Series 3 are not characterized by a major change in redox conditions within the depositional environment.

DOP values >0.75 have been recorded for limestone samples in the lower and upper parts of the Kaili Formation and could well reflect an iron deficiency frequently observed in carbonates. Fine-grained siliciclastic sediments reflect deposition largely under oxic conditions. In addition, the sulfur isotopic composition of sedimentary pyrite displays no correlation with DOP or with carbon and/or sulfur abundances and appears independent of lithology. With no evidence for prevailing anoxic bottom waters in the depositional environment, pyrite formation must have occurred in the sediment.

The sulfur isotopic composition of sedimentary pyrite displays a variation across the Cambrian Series 2 to Cambrian Series 3 that is broadly parallel for the two sections investigated in this study. In general, both sections display  $^{34}\text{S}$  enriched pyrite sulfur isotope values. Most pronounced is an excursion of approximately 10‰ towards less  $^{34}\text{S}$  enriched values just below the proposed boundary level. Comparably  $^{34}\text{S}$  enriched pyrite sulfur isotope values and a somewhat similar variation across this stratigraphic transition have been observed in other sections (Fig. 6), although differences in absolute values exist. These, however, likely reflect local/regional effects superimposed on a more globally representative variation in  $\delta^{34}\text{S}_{\text{pyrite}}$ .

The sulfur isotopic composition for sedimentary pyrite recorded in the Wuliu-Zengjiayan sections, and with less stratigraphic resolution also for the Jianshan section, displays an excursion towards less  $^{34}\text{S}$  enriched

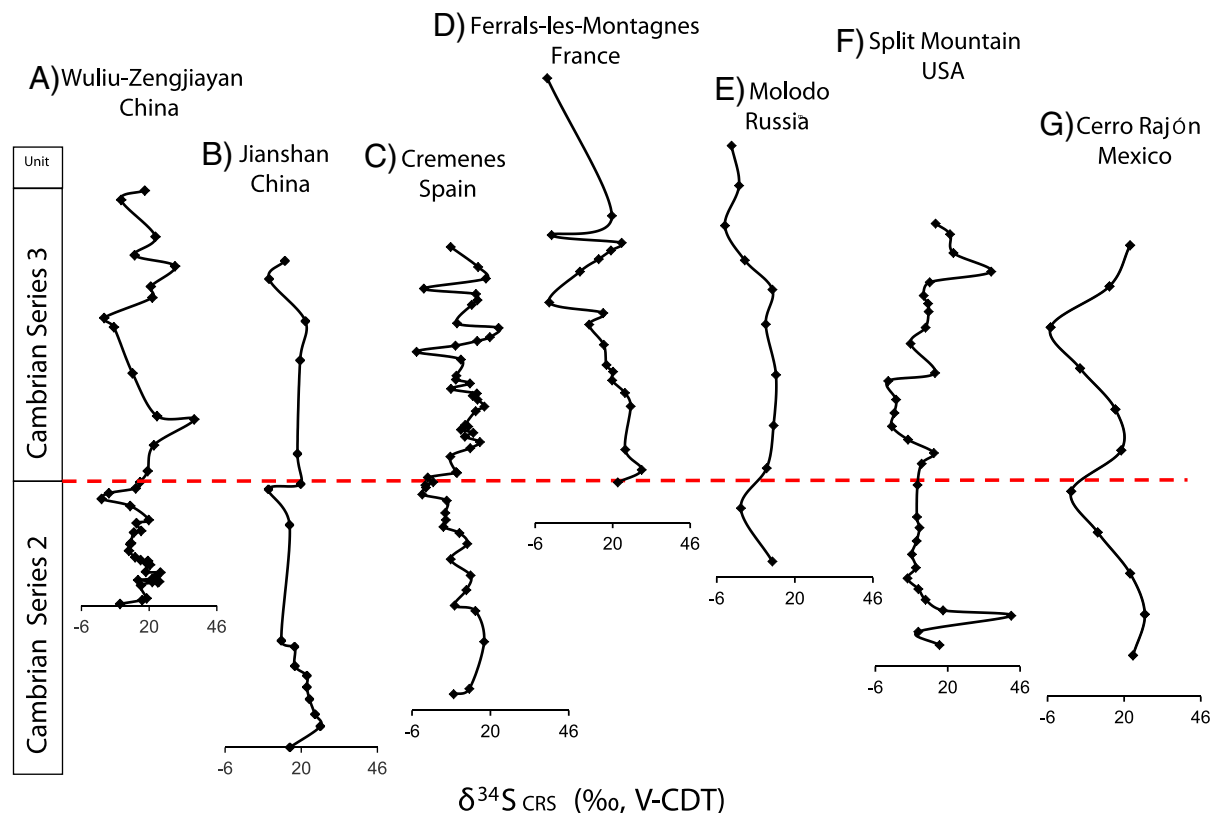


**Fig. 6.** Comparison of temporal variations in  $\delta^{34}\text{S}_{\text{CRS}}$  during the transition from Cambrian Series 2 to Cambrian Series 3 (A) Wuliu-Zengjiayan section (this study), (B) Jianshan section (this study), (C) Cremenes section (NW Spain; W-Gondwana) (Wotte et al., 2012), (D) Ferrals-les-Montagnes section (S-France; W-Gondwana) (Wotte et al., 2012), (E) Molodo River section (Siberian Platform) (Wotte et al., 2011), (F) Split Mountain section (Laurentia) (Wotte et al., 2011) and (G) Cerro Rajón section (Mexico; Laurentia) (Loyd et al., 2012).

values immediately preceding the Cambrian Series 2 to Cambrian Series 3 transition which is somewhat in phase with the evolution towards  $^{13}\text{C}$  depleted carbon isotope values (Figs. 3 and 4). Guo et al. (2010a) interpreted the negative carbon isotope excursion as a consequence of the transgressive flooding of the shelf with  $^{13}\text{C}$  depleted anoxic basinal waters. This influx of presumably anoxic bottom waters is not reflected in high DOP value of the respective samples. Without further data, the possible cause(s) remain speculative. HCl-soluble Fe, however, is rather high in the samples across the immediate boundary level which could suggest that the transgressive flooding delivered ferruginous rather sulfidic bottom waters. This would also be consistent with the low pyrite sulfur abundance in these samples.

## 6. Conclusions

The Cambrian Series 2 to Cambrian Series 3 transition archived by fine-grained siliciclastic sediments in the Wuliu-Zengjiayan and the Jianshan sections, Guizhou Province, South China, displays variable yet generally positive  $\delta^{34}\text{S}_{\text{pyrite}}$  values. An excursion towards less  $^{34}\text{S}$  enriched values immediately preceding the boundary intervals parallels the existing carbonate carbon isotope record for these sections. The proposed transgressive flooding with anoxic basinal waters during this stratigraphic interval is recorded by low rather than high DOP values which might indicate the delivery of ferruginous rather than sulfidic basinal waters onto the shelf area.

## Acknowledgments

Analytical work was performed at the Institute of Geologie und Paläontologie, Westfälische Wilhelms-Universität Münster, Germany. Artur Fugmann and Andreas Lutter are thanked for their help in the

laboratory. We wish to sincerely thank Dr. Zhu Maoyan, Dr. Robert R. Gaines, Dr. Jörg Maletz, Dr. Loren Babcock, and Dr. Frederick A. Sundberg for discussion and for assistance and expertise in the field and the laboratory. GQ acknowledges financial support by the One Hundred Talents Program of the Chinese Academy of Sciences, the Alexander Von Humboldt Foundation, the National Natural Science Foundation of China (NSFC Nos. 40972023, 40930211, 40902003, 41173008), the 973 Program (No. 2013CB835004), the Key Project of International Cooperation of Guizhou Science and Technology Department (No.2008-700110) and the National Commission on Stratigraphy of China (2013).

## References

- ASTM, 1977. Standard test methods for total sulfur in the analysis sample of coal and coke. Ann Book ASTM Standards, pp. 333–336.
- Brennan, S.T., Lowenstein, T.K., Horita, J., 2004. Seawater chemistry and the advent of biocalcification. *Geology* 32, 473–476.
- Calvert, S.E., Thode, H.G., Yeung, D., Karlin, R.E., 1996. A stable isotope study of pyrite formation in the Late Pleistocene and Holocene sediments of the Black Sea. *Geochim. Cosmochim. Acta* 60, 1261–1270.
- Canfield, D.E., 2001. Biogeochemistry of sulphur isotopes. In: Valley, J.W., Cole, D.R. (Eds.), *Stable Isotope Geochemistry*, pp. 607–633.
- Canfield, D., Raiswell, R., Westrich, J., Reaves, C., Berner, R., 1986. The use of chromium reduction in the analysis of inorganic sulfur in sediments and shales. *Chem. Geol.* 54, 149–155.
- Clark, L., Fritz, P., 1997. *Environmental Isotopes in Hydrogeology* [M]. Lewis Publisher, New York (328 pp.).
- Claypool, G.E., Holser, W.T., Kaplan, I.R., Sakai, H., Zak, I., 1980. The age curves of sulphur and oxygen isotopes in marine sulphate and their mutual interpretation. *Chem. Geol.* 28, 199–260.
- Fike, D.A., Grotzinger, J.P., 2008. A paired sulphate–pyrite d $^{34}\text{S}$  approach to understanding the evolution of the Ediacaran–Cambrian sulphur cycle. *Geochim. Cosmochim. Acta* 72, 2636–2648.
- Gaines, R.R., Hammarlund, E.U., Hou, X.G., Qi, C., Gabbott, S.E., Zhao, Y.L., Peng, J., Canfield, D.E., 2012. Mechanism for Burgess Shale-type preservation. *Proc. Natl. Acad. Sci.* 109, 5180–5184.

- Gill, B.C., Lyons, T.W., Saltzman, M.R., 2007. Parallel, high-resolution carbon and sulphur isotope records of the evolving Paleozoic marine sulphur reservoir. *Palaeogeogr. Palaeoclimatol. Palaeoecol.* 256, 156–173.
- Gill, B.C., Lyons, T.W., Young, S.A., Kump, L.R., Knoll, A.H., Saltzman, M.R., 2011. Geochemical evidence for widespread euxinia in the later Cambrian Ocean. *Nature* 469, 80–83.
- Goldberg, T., Poulton, S.W., Strauss, H., 2005. Sulphur and oxygen isotope signatures of late Neoproterozoic to early Cambrian sulphate, Yangtze Platform, China: diagenetic constraints and seawater evolution. *Precambrian Res.* 137, 223–241.
- Goldberg, T., Strauss, H., Guo, Q., Liu, C., 2007. Reconstructing marine redox conditions for the Early Cambrian Yangtze Platform: evidence from biogenic sulfur and organic carbon isotopes. *Palaeogeogr. Palaeoclimatol. Palaeoecol.* 254, 175–193.
- Guo, Q., Strauss, H., Liu, C., Zhao, Y., Pi, D., Fu, P., Zhu, L., Yuan, J., 2005. Carbon and oxygen isotopic composition of Lower to Middle Cambrian sediments at Taijiang, Guizhou Province, China. *Geol. Mag.* 142, 723–733.
- Guo, Q., Strauss, H., Kaufman, A.J., Schröder, S., Gutzmer, J., Wing, B., Baker, M.A., Bekker, A., Jin, Q., Kim, S.-T., Farquhar, J., 2009. Reconstructing Earth's surface oxidation across the Archean–Proterozoic transition. *Geology* 37 (5), 399–402.
- Guo, Q., Strauss, H., Liu, C., Zhao, Y., Yang, X., Peng, J., Yang, H., 2010a. A negative carbon isotope excursion defines the transition from Cambrian Series 2 to Cambrian Series 3 on the Yangtze Platform, South China. *Palaeogeogr. Palaeoclimatol. Palaeoecol.* 285, 143–151.
- Guo, Q., Strauss, H., Liu, C., Zhao, Y., Yang, X., Peng, J., Yang, H., 2010b. Corrigendum to “A negative carbon isotope excursion defines the boundary from Cambrian Series 2 to Cambrian Series 3 on the Yangtze Platform, South China”. *Palaeogeogr. Palaeoclimatol. Palaeoecol.* 285, 143–151 (Palaeogeography, Palaeoclimatology, Palaeoecology 288, 118).
- Habicht, K.S., Canfield, D.E., Rethmeyer, J., 1998. Sulphur isotope fractionation during bacterial sulfate reduction and disproportionation of thiosulfate and sulphite. *Geochim. Cosmochim. Acta* 62, 2585–2595.
- Halverson, G.P., Hurtgen, M.T., 2007. Ediacaran growth of the marine sulfate reservoir. *Earth Planet. Sci. Lett.* 263, 32–44.
- Hough, M.L., Shields, G.A., Evins, L.Z., Strauss, H., Henderson, R.A., Mackenzie, S., 2006. A major sulfur isotope event at 510 Ma: a possible anoxia-extinction-volcanism connection during the Early–Middle Cambrian transition? *Terra Nova* 18, 257–263.
- Hurtgen, M.T., Halverson, G.P., Arthur, M.A., Hoffman, P.F., 2006. Sulfur cycling in the aftermath of a 635-Ma snowball glaciation: evidence for a syn-glacial sulfidic deep ocean. *Earth Planet. Sci. Lett.* 245, 551–570.
- Hurtgen, M.T., Pruss, S.B., Knoll, A.H., 2009. Evaluating the relationship between the carbon and sulphur cycles in the later Cambrian ocean: an example from the Port au Port Group, western Newfoundland, Canada. *Earth Planet. Sci. Lett.* 281, 288–297.
- Johnston, D.T., 2011. Multiple sulfur isotopes and the evolution of Earth's surface sulfur cycle. *Earth-Sci. Rev.* 106, 161.
- Kampschulte, A., Strauss, H., 2004. The sulphur isotopic evolution of Phanerozoic seawater based on the analysis of structurally substituted sulphate in carbonates. *Chem. Geol.* 204, 255–286.
- Kampschulte, A., Bruckschen, P., Strauss, H., 2001. The sulphur isotopic composition of trace sulphates in Carboniferous brachiopods: implications for coeval seawater, correlation with other geochemical cycles and isotope stratigraphy. *Chem. Geol.* 175, 149–173.
- Kaufman, A.J., Sial, A.N., Frimmel, H.E., Misi, A., 2009. Neoproterozoic to Cambrian palaeoclimatic events in southwestern Gondwana. *Precambrian Geol.* 16, 388–669.
- Kouchinsky, A., Bengtson, S., Gallet, Y., Korovnikov, I.V., Pavlov, V., Runnegar, B., Shields, G.A., Veizer, J., Young, E., Ziegler, K., 2008. The SPICE carbon excursion in Siberia: a combined study of the upper Middle Cambrian–lowermost Ordovician Kulyumbe River section, northwestern Siberian Platform. *Geol. Mag.* 145, 609–622.
- Loyd, S.J., Marenco, P.J., Hagadorn, J.W., Lyons, T.W., Kaufman, A.J., Sour-Tovar, F., Corsetti, F.A., 2012. Sustained low marine sulfate concentrations from the Neoproterozoic to the Cambrian: insights from carbonates of northwestern Mexico and eastern California. *Earth Planet. Sci. Lett.* 339–340, 79–94.
- Lyons, T.W., Werne, J.P., Hollander, D.J., Murray, R.W., 2003. Contrasting sulfur geochemistry and Fe/Al and Mo/Al ratios across the last oxic-to-anoxic transition in the Cariaco Basin, Venezuela. *Chem. Geol.* 195, 131–157.
- Montanez, J.P., Osleger, D.A., Banner, J.L., Mack, L.E., Masgrove, M.L., 2000. Evolution of the Sr and C isotope composition of Cambrian oceans. *GSA Today* 10, 1–7.
- Raiswell, R., Buckley, F., Berner, R., Anderson, T., 1988. Degree of pyritization of iron as a paleoenvironmental indicator of bottomwater oxygenation. *J. Sediment. Petrol.* 58, 812–819.
- Reuschel, M., Melezhik, V.A., Lepland, A., Fallick, A.E., Strauss, H., 2012. Isotopic evidence for a sizeable seawater sulfate reservoir at 2.1 Ga. *Precambrian Res.* 192, 78–88.
- Ries, J.B., Fike, D.A., Pratt, L.M., Lyons, T.W., Grotzinger, J.P., 2009. Superheavy pyrite ( $\delta^{34}\text{S}_{\text{Py}} > \delta^{34}\text{S}_{\text{SCS}}$ ) in the terminal Proterozoic Nama Group, southern Namibia; a consequence of low seawater sulfate at the dawn of animal life. *Geology* 37, 743–746.
- Saltzman, M.R., Ripperdan, R.L., Brasier, M.D., Lohmann, K.C., Robison, R.C., Chang, W.T., Peng, S., Ergaliev, E.K., Runnegar, B.R., 2000. A global carbon isotope excursion (SPICE) during the Late Cambrian: relation to trilobite extinction, organic-matter burial, and sea level. *Palaeogeogr. Palaeoclimatol. Palaeoecol.* 160, 211–223.
- Scotes, C.R., McKerrow, W.S., 1990. Revised world maps and introduction. *Geol. Soc. Lond. Mem.* 12, 1–21.
- Shields, G.A., Strauss, H., Howe, S.S., Siegmund, H., 1999. Sulphur isotope composition of sedimentary phosphorites from the basal Cambrian of China: implications for Neoproterozoic–Cambrian biogeochemical cycling. *J. Geol. Soc. Lond.* 156, 943–955.
- Shields, G.A., Kimura, H., Yang, J., Gammon, P., 2004. Sulphur isotopic evolution of Neoproterozoic–Cambrian seawater: new francolite-bound sulphate  $\delta^{34}\text{S}_{\text{SCS}}$  data and a critical appraisal of the existing record. *Chem. Geol.* 204, 163–182.
- Sim, M.S., Bosak, T., Ono, S., 2011. Large sulfur isotope fractionation does not require disproportionation. *Science* 333, 74–77.
- Strauss, H., 1999. Geological evolution from isotope proxy signals – sulfur. *Chem. Geol.* 161, 89–101.
- Strauss, H., 2004. 4 Ga of seawater evolution: evidence from the sulphur isotopic composition of sulphate. In: Amend, J.P., Edwards, K.J., Lyons, T.W. (Eds.), *Sulphur Biogeochemistry – Past and Present*. Geological Society of America, Boulder, pp. 195–205.
- Strauss, H., Melezhik, V.A., Reuschel, M., Fallick, A.E., Lepland, A., Rychanchik, D.V., 2013. Abundant marine calcium sulphates – radical change of seawater sulphate reservoir and sulphur cycle. In: Melezhik, V.A., Prave, A.R., Fallick, A.E., Kump, L.R., Strauss, H., Lepland, A., Hanski, E.J. (Eds.), *Reading the Archive of Earth's Oxygenation. Global Events and the Fennoscandian Arctic Russia – Drilling Early Earth Project*, vol. 3 (Chapter 7.5).
- Sundberg, F.A., Yuan, J., McCollum, L.B., Zhao, Y., 1999. Correlation of the Lower–Middle Cambrian boundary of South China and Western United States of America. *Acta Palaeontol. Sin.* 38, 102–107.
- Sundberg, F.A., Zhao, Y., Yuan, J., Lin, J., 2011. Detailed trilobite biostratigraphy across the proposed GSSP for Stage 5 (“Middle Cambrian” boundary) at the Wuliu-Zengjiayan section, Guizhou, China. *Bull. Geosci.* 86 (3), 423–464.
- Wotte, T., Strauss, H., Sundberg, F.A., 2011. Carbon and sulfur isotopes from the Cambrian Series 2–Cambrian Series 3 of Laurentia and Siberia. In: Hollingsworth, J.S., Sundberg, F.A., Foster, J.R. (Eds.), *Museum of Northern Arizona Bulletin*, 67, p. 43na.
- Wotte, T., Strauss, H., Fugmann, A., Garbe-Schoenberg, D., 2012. Paired  $\delta^{34}\text{S}$  data from carbonate-associated sulfate and chromium-reducible sulfur across the traditional Lower–Middle Cambrian boundary of W-Gondwana. *Geochim. Cosmochim. Acta* 85, 228–253.
- Zhang, Z., Shen, J., Gong, X., Zhao, Y., 1996. A preliminary discussion on preservation condition of Kaili Fauna, Middle Cambrian, Taijiang, Guizhou. *Acta Palaeontol. Sin.* 35 (5), 607–622.
- Zhao, Y., Yuan, J., Zhu, L., Guo, Q., Yang, R., Yang, X., 2001a. A progress report on research and prospects of the Lower–Middle Cambrian boundary in China. *J. Stratigr.* 25, 376–383.
- Zhao, Y., Yuan, J., McCullum, L.B., Sundberg, F.A., Yang, R., Guo, Q., Zhu, L., Yang, X., 2001b. A potential GSSP for the Lower and Middle Cambrian boundary near Balang village, Taijiang county, Guizhou Province, China. *Acta Palaeontol. Sin.* 40, 130–142.
- Zhao, Y., Yuan, J., Peng, S., Loren, E.B., Peng, J., Lin, J., Guo, Q., 2007. New data on the Wuliu-Zengjiayan section (Balang, South China), GSSP candidate for the base of Cambrian Series 3. *Mem. Assoc. Australas. Palaeontol.* 33, 57–65.
- Zhao, Y., Yuan, J., Peng, S., Loren, E.B., Peng, J., Guo, Q., Lin, J., Tai, T., Yang, R., Wang, Y., 2008. A new section of Kaili Formation (Cambrian) and a biostratigraphic study of the boundary interval across the undefined Cambrian Series 2 and Series 3 at Jianshan, Chuandong village, Jianhe County, China with a discussion of global correlation based on the first appearance datum of *Oryctocephalus indicus* (Reed, 1910). *Prog. Nat. Sci.* 18, 1549–1556.
- Zhao, Y., Peng, J., Yuang, J., Guo, Q., Tai, T., Yin, L., Parsley, R.L., Yang, Y., Yang, X., Zhang, P., 2012. The Kaili Formation and Kaili Biota at the Wuliu-Zengjiayan Section of Guizhou Province, China and proposed Global Standard Stratotype Section and Point (GSSP) of the unnamed Cambrian Series 3, Stage 5. The 17th Field Conference of the Cambrian Stage Subdivision Working Group, International Subcommission on Cambrian Stratigraphy and Celebration of the 30th Anniversary of the Discovery of the Kaili Biota. Guizhou Univ. (Suppl. 1), 108–124.